Experimental evidence for crustal control over seismic fault segmentation

M. Lefevre, P. Souloumiac, N. Cubas, Y. Klinger

▶ **To cite this version:**

M. Lefevre, P. Souloumiac, N. Cubas, Y. Klinger. Experimental evidence for crustal control over seismic fault segmentation. Geology, 2020, 48 (8), pp.844-848. 10.1130/G47115.1 . hal-03063897

HAL Id: hal-03063897
https://hal.science/hal-03063897

Submitted on 14 Dec 2020

HAL is a multi-disciplinary open access archive for the deposit and dissemination of scientific research documents, whether they are published or not. The documents may come from teaching and research institutions in France or abroad, or from public or private research centers.

L'archive ouverte pluridisciplinaire **HAL**, est destinée au dépôt et à la diffusion de documents scientifiques de niveau recherche, publiés ou non, émanant des établissements d'enseignement et de recherche français ou étrangers, des laboratoires publics ou privés.

Experimental evidence for crustal control over seismic fault segmentation

Lefevre[1*] M., Souloumiac[2] P., Cubas[3] N., Klinger[1*] Y.

1: Université de Paris, Institut de physique du globe de Paris, CNRS, F-75005 Paris, France

2: GEC, Université de Cergy-Pontoise, F-95000 Neuville sur Oise, France

3: Sorbonne Université, ISTEP, F-75005 Paris, France

marthe.lefevre1@gmail.com

ABSTRACT

Strike-slip faults are described as continuous structures, while they are actually formed of successive segments separated by geometrical complexities. Although this along-strike segmentation is known to affect the overall dynamics of earthquakes, the physical processes governing the scale of this segmentation remain unclear. Here, we use analogue models to investigate the structural development of strike-slip faults and the physical parameters controlling segmentation. We show that length of fault segments is regular along strike, and scales linearly with the thickness of the brittle material. Variations of the rheological properties only have minor effects on the scaling relationship. Ratios between the segment length and the brittle material thickness are similar for co-seismic ruptures and sandbox experiments. This supports a model where crustal seismogenic thickness controls fault geometry. Finally, we show that the

geometrical complexity acquired during the strike-slip fault formation withstands cumulative displacement. Thus, inherited complexity impedes the formation of an ever straighter fault, and might control the length of earthquakes ruptures.

INTRODUCTION

Strike-slip faults are discontinuous features formed by a succession of segments, separated by geometrical complexities, such as bends, or relay zones (Fig. 1.a, S1)(e.g. Segall and Pollard, 1980). Although the size of these complexities is highly variable, even the smaller ones can significantly affect initiation, propagation, and termination of earthquakes (e.g. King and Nabelek, 1985; Wesnousky, 2006; Klinger et al., 2005; Manighetti et al., 2007), implying their persistence at seismogenic depth (e.g. Schwartz and Coppersmith, 1984; Wei et al., 2011; Schwartz, 2018). Fault discontinuities also modulate amplitude and style of co-seismic surface deformation (Klinger et al., 2006; Vallée et al., 2008), and might stop ruptures propagation if larger than 5 km (e.g. Wesnousky, 2006). Recently, numerical simulations of rupture scenarios have confirmed the strong dependency of earthquake rupture models on the geometry of the fault system (e.g. Aochi and Ulrich, 2015; Lozos, 2016; Klinger et al., 2018). As a consequence, understanding the genesis of the segmentation and its scaling is critical for physics-based earthquake modeling, as well as for hazard assessment, since complexities impact the earthquake rupture length, and thus its magnitude.

Based on experimental, seismological, and geomorphological studies, fault segmentation was first described as fractal (e.g. Aviles et al., 1987; Okubo and Aki, 1987). Alternatively, it was suggested that faults are composed of a fixed number of segments, implying a segment length varying between faults (e.g. Manighetti et al., 2015).

Conversely, studies based on co-seismic rupture maps have argued in favor of a constant segment length of about 18 km ± 5 km, independent of the regional tectonic setting or the earthquake magnitude, suggesting an external controlling factor, which is assumed to be the seismogenic crust thickness (e.g. Bilham and Williams, 1985; Klinger, 2010)(Fig. 1.a). However, detailed co-seismic rupture maps are available only for a limited number of earthquakes, preventing a reliable statistical analysis. The lack of data combined with our limited knowledge of the fault segmentation process prevent us from discriminating between these models.

To tackle the origin of strike-slip fault segmentation, we followed an analogue modeling approach, which provides the complete geometrical evolution of the fault structure while accumulating slip. Moreover, a large number of experiments can be conducted, allowing for a thorough exploration of the impact of the geometrical and rheological parameters.

ANALOGUE MODELING OF STRIKE-SLIP FAULTS

Numerous analogue studies already focused on the formation and final geometry of strike-slip faults systems (Dooley and Schreurs, 2012 and references therein). In experiments with sand overlying a straight basal dislocation, the first structures to appear are the Riedel shears (R-shears)(Riedel, 1929; Naylor et al., 1986), propagating upward (e.g. Ueta et al., 2000, Cambonie et al., 2018), oriented at the surface at an angle of $\varphi_{int}/2$ relative to strike-slip basal fault (φ_{int}, angle of internal friction of the material). This orientation is due to the helicoidal shape of the Riedels (Fig 1,b) (Naylor et al., 1986; Mandl, 1987). The next structures to appear are first, synthetic shears (S-shear) that only slightly deviate from the strike of the basal fault, and finally P-shears, which cross the basal fault in the opposite direction. Eventually, coalescence of these different

shears leads to the formation of an anastomosed fault zone (e.g. Naylor et al., 1986; Richard et al., 1995).

Here, we investigate if the first structures to appear during the formation of strike-slip faults can be responsible for the long-term segmentation. As these faults result from the linkage of the S-shears, the initial discontinuities between them at the locations of the Riedels might persist and give rise to geometrical complexities. Therefore, we consider the distance between two adjacent Riedels as equivalent to a fault segment. Although dependency of the length of Riedels on the thickness of the frictional material had already been suspected, it was never indisputably demonstrated (Tchalenko, 1970; Atmaoui et al., 2006, Hatem et al., 2017). Thus, we first evaluate the influence of the material thickness on the inter-Riedels distance, and then the impact of intrinsic properties of the material.

We used an analogue model set-up known as Riedel experiments in a 1.2m x 0.8m box (detailed set-up in Supp. Mat., Fig. S2). The model reproduces brittle deformation in a non-cohesive material during the onset of a strike-slip fault in a homogeneous sandpack above a straight-basal fault. To test the impact of the frictional properties on the fault geometry, we used four different Aeolian sands with different internal frictions (Sand 1, φ_{int}=43.7°; Sand 2, φ_{int}=35.6°; Sand 3, φ_{int}=33.4°; Sand 4, φ_{int}=22.1°) and variable basal materials, such as PVC (φ_b=13°) Alkor-foil (φ_b=18°) and sand paper (φ_b>43,7°). Some of these sands are poured and have a rate-hardening behavior (sand 2, 3 and 4), while sand 1 is sedimented and rate-weakening (see Supp. Mat. for material properties). A camera placed above the box records the deformation every 0.5mm of basal displacement to generate orthoimages of the sandbox surface, with a resolution of the order of the grain size. Moreover, to assess how the shear is accommodated by the different structures, we computed the incremental displacement field from optical images correlation using

Micmac software (Rosu et al., 2015). The set-up is intentionally simple to limit the number of free parameters and to ensure a good control on the boundary conditions of the experiment. The aim of these experiments is not to reproduce details of a realistic strike-slip fault evolution, but to retrieve relationships between fault-characteristic patterns and properties of material.

For each sandpack thickness (T), three parameters were extracted from surface images for each Riedel: the inter-Riedel distances (S) measured parallel to the trace of the basal fault, the Riedels length (L), and the angle (α) formed by the Riedel with the direction of the basal fault (Fig. 1.c). We ran repeated experiments with thicknesses varying from 2 to 5 cm (Table S1). Only the experiments with thicknesses lower or equal to 5cm were free of edge effects (Fig. S3). The minimum thickness is constrained by the ability of the sand to develop the 3D helicoidal shape of Riedel shears. When sand is thinner than 1.5 cm, instead of the Riedel shears, a continuous fault directly appears at the surface (Fig. S4).

To provide robust correlations between thickness, material properties, and fault geometry, we need repeated experimental measurements. As several Riedels are visible in each experiment, we checked that we could use them as independent measurements to improve statistical significance (see verification in Supp. Mat.). In the following, for clarity's sake, only average quantities per experiment are presented and discussed (individual measurements in Supp. Mat. Fig. S7-S11).

SCALING RELATIONSHIPS DERIVED FROM SANDBOX

Surface images of the experiments for different thicknesses (T) show that the deformed area widens and the inter-Riedel distance (S) increases for thicker sandpack (Fig. 2.a).

121 Indeed, systematic measurements of (S) for different (T) show a linear correlation
122 between those parameters (Fig. 2.b), with a scale factor of about 2.8 for Sand 1.
123 To test the potential effect of the material properties, we first performed experiments
124 with sands of different internal friction. The three sets of experiments exhibit the same
125 trend: (S) increases with (T)(Fig. 2.c, S7), and the measurements distributions are well
126 modeled by linear relationships. Nevertheless, depending on the internal friction, the
127 slope of the best-fit lines changes, indicating a partial control of the material properties
128 on the size of the structures. The slope is 1.43 for the smaller friction (ϕ_{int}=33.4°, Sand
129 3), 1,61 for the intermediate friction (ϕ_{int}=35.6°, Sand 2), and 2.76 for the highest one
130 (ϕ_{int}=43.7°, Sand 1). As Sand 2 and 3 present relatively similar relationships (Fig. 2.c)
131 and are both strain-hardening, we cannot exclude from our data that the discrepancy
132 between Sand 1 and other sands could be due to its strain-weakening properties instead
133 of its internal friction (Fig. S11). Nevertheless, as Riedel shears form when shear stress
134 reaches the static friction (Tchalencko, 1970, Ritter et al. 2018), we think that the
135 internal friction, of the sands controls the relation between S and T, and not its strain
136 hardening or weakening property.
137 Using different materials to test the impact of the internal friction might also change the
138 basal friction between the different experiments. To assess a possible trade-off between
139 these two parameters, we conducted three series of experiments using Sand 1 with
140 different basal materials (Fig. 2.d, S7). For the three tested basal frictions we observed
141 linear relations between (S) and (T). The slopes of the regressions are quite similar, and
142 only the intercepts change slightly (Fig. 2.d). The associated change of x-axis intercept
143 corresponds to the minimal thickness necessary to develop the Riedels-helicoid. This
144 observation suggests that the basal friction impacts the formation of the helicoid,

145 probably by changing the width of the deformed area at depth (see Supp. Mat.
146 mechanical implications).
147 We then examined the effect of the cohesion on the inter-Riedel distance (S), using non-
148 cohesive (Sand 3) and strongly cohesive (Sand 4) sands (Fig. 2.e, S8). Again, (S)
149 increases linearly with (T). The two linear regressions present the same slope but
150 shifted intercepts, with a larger value for the highly cohesive sand (of about 1.5 cm).
151 However, this difference may not be significant in view of the small number of
152 experiments associated to a high dispersion of the Sand 4 measurements, interpreted as
153 resulting from heterogeneities in the sand mixture due to its electro-static charge (see
154 Supp. Mat.). We consider that cohesion only marginally affects the fault geometry, as (S)
155 is only slightly affected whereas all parameters vary and uncertainties are significant.

156 **COMPARISON OF EXPERIMENTAL RESULTS WITH EARTHQUAKE SURFACE-**
157 **RUPTURES GEOMETRY**

158 This new set of experiments demonstrates unambiguously that the inter-Riedel distance
159 (S) is directly controlled by the thickness of the sandpack (T)(Fig. 2), while the material
160 properties have secondary effects. The internal friction controls the scaling factor of the
161 linear relation between (S) and (T), whereas the basal friction and the cohesion only
162 marginally impact this relation. The width and rheology of the basal deformation zone,
163 which are not addressed here, might also affect the size of structures (Hatem et al. 2017,
164 Zuza et al. 2017, Yang et al. 2020).
165 According to field studies, strike-slip fault segments, measured between two successive
166 relay zones, have similar lengths independently of the local tectonic setting (Klinger,
167 2010). Thus, it was suggested that the average length of fault segments scales with the
168 thickness of the seismogenic crust (Bilham and Williams, 1985; Klinger, 2010), with a

ratio close to 1. To compare our experiments with natural observations, we selected sands 2 and 3, both non-dilatant and with frictions within the same range as standard upper crust materials ($\mu \sim 0.7$)(e.g. Byerlee, 1978).

For comparison, the inter-Riedel distance and the length of fault segments were normalized respectively by the thickness of sand and of seismogenic crust, which is derived from the literature (details in Supp. Mat.). The average normalized length for natural fault segments is 1.16, and for sands 2 and 3 it is 1.17 and 1.3, which are indistinguishable from the natural case (Fig. 3). Moreover, individual ratio values are all in a narrow range (σ=0.43), which indicates that such similarity is not coincidental. This supports the hypothesis that the length of continental strike-slip segments is directly controlled by the thickness of the seismogenic crust.

Although this approach does not capture the effects of a dynamic rupture, it sheds light upon the way faults sections grow to eventually coalesce into an apparent continuous structure. Interestingly, our experiments show that even when the cumulative displacement during the experiment starts to be large enough to dismantle the Riedels and to allow coalescence of successive S-shears into a longer fault, the initial geometric discontinuity related to the location of the Riedel is preserved (Fig. 4.a). Riedels act as inherited faults influencing the location of subsequent deformation. In the case of strike-slip faults, such discontinuities will turn into relay zones, either compressional or extensional. Indeed, in nature faults form in crust that already went through multiple stages of deformation and that displays local geological variation. Thus the simple scenario of faults structured only according to the thickness of the brittle crust is likely modulated by inherited crustal heterogeneities, resulting in some relay zones being larger than others. Sandbox experiments can also present such variability with larger complexities randomly appearing (Fig. S14), suggesting that the initial orientation of the

S-shears might also influence the size of the relay zones. Other studies have proposed that the off-fault deformation of earthquakes could be related to the reactivation of these Riedels (Hatem et al. 2017), although we could not observe such reactivation in our experiments. Moreover, in nature evidence of the initial Riedels structures is tenuous, as they accommodate a very short amount of deformation before being passively offset by the main active fault, which explains their weak morphological expression at the surface. These results show that the first stages of deformation determine the long-term scaling of the of strike-slip faults segmentation: Riedels create a regular pattern of geometrical complexities, which is inherited throughout the fault history (Fig. 4.b). This pattern of segmentation does not seem to experience significant changes even after the Riedels have ceased to be active, as we keep seeing it on the coseismic-rupture map. Thus, this questions the paradigm that faults become even more linear while accumulating displacement through time, and thus prone to larger earthquakes. Instead, strike-slip fault geometry may retain a constant level of complexity, which controls the size of earthquakes.

REFERENCES

Aochi, H., and Ulrich, T., 2015, A probable earthquake scenario near Istanbul determined from dynamic simulations: Bulletin of the Seismological Society of America, v. 105, no. 3, p. 1468–1475, doi: 10.1785/0120140283>.

Atmaoui, N., Kukowski, N., Stöckhert, B., and König, D., 2006, Initiation and development of pull-apart basins with Riedel shear mechanism: insights from scaled clay experiments: International Journal of Earth Sciences, v. 95, no. 2, p. 225–238, doi: 10.1007/s00531-005-0030-1.

Aviles, C.A., Scholz, C.H., and Boatwright, J., 1987, Fractal analysis applied to characteristic segments of the San Andreas Fault: Journal of Geophysical Research: Solid Earth, v. 92, no. B1, p. 331–344, doi: 10.1029/JB092iB01p00331.

Bilham, R., and Williams, P., 1985, Sawtooth segmentation and deformation processes on the southern San Andreas fault, California: Geophysical Research Letters, v. 12, no. 9, p. 557–560.

Byerlee, J., 1978, Friction of Rocks, *in* Rock Friction and Earthquake Prediction, Birkhäuser, Basel, Basel, p. 615–626.

Cambonie, T., Klinger, Y., & Lazarus, V., 2019, Similarities between mode III crack growth patterns and strike-slip faults : Philosophical Transactions of the Royal Society A, v. 377, no. 2136, p. 20170392.

Dooley, T.P., and Schreurs, G., 2012, Analogue modelling of intraplate strike-slip tectonics: A review and new experimental results: Tectonophysics, v. 574-575, no. C, p. 1–71, doi: 10.1016/j.tecto.2012.05.030.

Hatem, A.E., Cooke, M.L., Toeneboehn, K., 2017, Strain localization and evolving kinematic efficiency of initiating strike-slip faults within wet kaolin experiments: Journal of Structural Geology, v. 101, p. 96–108, doi: 10.1016/j.jsg.2017.06.011.

King, G., and Nabelek, J., 1985, Role of fault bends in the initiation and termination of earthquake rupture.: Science, v. 228, no. 4702, p. 984–987, doi: 10.1126/science.228.4702.984.

Klinger, Y., 2010, Relation between continental strike-slip earthquake segmentation and thickness of the crust: Journal of Geophysical Research, v. 115, no. B7, p. 1355–19, doi: 10.1029/2009JB006550.

Klinger, Y., Michel, R., and King, G., 2006, Evidence for an earthquake barrier model from Mw~7.8 Kokoxili (Tibet) earthquake slip-distribution: Earth and Planetary Science Letters, v. 242, no. 3-4, p. 354–364, doi: 10.1016/j.epsl.2005.12.003.

Klinger, Y., Okubo, K., Vallage, A., Champenois, J., Delorme, A., Rougier, E., Lei, Z., Knight, E.E., Munjiza, A., Satriano, C., Baize, S., Langridge, R., and Bhat, H.S., 2018, Earthquake Damage Patterns Resolve Complex Rupture Processes: Geophysical Research Letters, v. 45, no. 19, p. 10,279–10,287, doi: 10.1029/2018GL078842.

Klinger, Y., Xu, X., and Tapponnier, P., 2005, High-resolution satellite imagery mapping of the surface rupture and slip distribution of the Mw~ 7.8, 14 November 2001 Kokoxili earthquake, Kunlun fault, northern Tibet, China: Bulletin of the Seismological Society of America, v. 95, no. 5, p. 19770–11987, doi: 10.1785/0120040233.

Lauer, B., Grandin, R., Klinger, Y., Vallage, A., Jolivet, R., and Delorme, A., 2018, Absence of shallow slip deficit during the Balochistan earthquake (2013, Mw 7.7, Pakistan): insights from SAR and optical-based coseismic slip model: AGU Fall Meeting.

Lozos, J.C., 2016, A case for historic joint rupture of the San Andreas and San Jacinto faults: Science Advances, v. 2, no. 3, p. e1500621–8, doi: 10.1126/sciadv.1500621.

Mandl, G., 1987, Discontinuous fault zones: Journal of Structural Geology, v. 9, no. 1, p. 105–110, doi: 10.1016/0191-8141(87)90047-2.

Manighetti, I., Campillo, M., Bouley, S., and Cotton, F., 2007, Earthquake scaling, fault segmentation, and structural maturity: Earth and Planetary Science Letters, v. 253, no. 3-4, p. 429–438, doi: 10.1016/j.epsl.2006.11.004.

263 Manighetti, I., Caulet, C., De Barros, L., Perrin, C., Cappa, F., and Gaudemer, Y., 2015,
264 Generic along-strike segmentation of Afar normal faults, East Africa: Implications on
265 fault growth and stress heterogeneity on seismogenic fault planes: Geochemistry,
266 Geophysics, Geosystems, v. 16, no. 2, p. 443–467, doi: 10.1002/2014GC005691.

267 Naylor, M.A., Mandl, G.T., and Supesteijn, C., 1986, Fault geometries in basement-induced
268 wrench faulting under different initial stress states: Journal of Structural Geology, v. 8,
269 no. 7, p. 737–752.

270 Okubo, P.G., and Aki, K., 1987, Fractal geometry in the San Andreas Fault System: Journal
271 of Geophysical Research: Solid Earth, v. 92, no. B1, p. 345–355, doi:
272 10.1029/JB092iB01p00345.

273 Richard, P.D., Naylor, M.A., and Koopman, A., 1995, Experimental models of strike-slip
274 tectonics: Petroleum Geoscience, v. 1, no. 1, p. 71–80, doi: 10.1144/petgeo.1.1.71.

275 Riedel, W., 1929, Zur Mechanik geologischer Brucherscheinungen ein Beitrag zum
276 Problem der Fiederspatten.: Zentbl. Miner. Geol. Palaont. Abt,, p. 354–368.

277 Ritter, M. C., Rosenau, M., & Oncken, O., 2018, Growing faults in the lab: Insights into the
278 scale dependence of the fault zone evolution process : Tectonics, v. 37 , no. 1, p. 140-153,
279 doi : 10.1016/j.tecto.2017.11.018.
280
281 Rosu, A.-M., Pierrot-Deseilligny, M., Delorme, A., Binet, R., and Klinger, Y., 2015,
282 Measurement of ground displacement from optical satellite image correlation using the
283 free open-source software MicMac: ISPRS Journal of Photogrammetry and Remote
284 Sensing, v. 100, no. C, p. 48–59, doi: 10.1016/j.isprsjprs.2014.03.002.

285 Schwartz, D.P., 2018, Review: Past and Future Fault Rupture Lengths in Seismic Source
286 Characterization—The Long and Short of It: Bulletin of the Seismological Society of
287 America, v. 108, no. 5A, p. 2493–2520, doi: 10.1785/0120160110.

288 Schwartz, D.P., and Coppersmith, K.J., 1984, Fault behavior and characteristic
289 earthquakes' examples from the Wasatch and San Andreas fault zones : Journal of
290 Geophysical Research, v. 89, no. B7, p. 5681–5698.

291 Segall, P., and Pollard, D.D., 1980, Mechanics of discontinuous faults: Journal of
292 Geophysical Research: Solid Earth, v. 85, no. B8, p. 4337–4350, doi:
293 10.1029/JB085iB08p04337.

294 Tchalenko, J.S., 1970, Similarities between shear zones of different magnitudes:
295 Geological Society of America Bulletin.

296 Ueta, K., Tani, K., Geology, T.K.E., 2000, Computerized X-ray tomography analysis of
297 three-dimensional fault geometries in basement-induced wrench faulting: Elsevier, v. 56,
298 no. 1-2, p. 197–210, doi: 10.1016/S0013-7952(99)00143-X.

299 Vallée, M., Landès, M., Shapiro, N.M., and Klinger, Y., 2008, The 14 November 2001
300 Kokoxili (Tibet) earthquake: High-frequency seismic radiation originating from the
301 transitions between sub-Rayleigh and supershear rupture velocity regimes: Journal of
302 Geophysical Research, v. 113, no. B7, p. 2064–14, doi: 10.1029/2007JB005520.

Wei, S., Fielding, E., Leprince, S., Sladen, A., Avouac, J.P., Helmberger, D., Hauksson, E., Chu, R., Simons, M., Hudnut, K., Herring, T., and Briggs, R., 2011, Superficial simplicity of the 2010 El Mayor–Cucapah earthquake of Baja California in Mexico: Nature Geoscience, v. 4, no. 9, p. 615–618, doi: 10.1038/ngeo1213.

Wesnousky, S.G., 2006, Predicting the endpoints of earthquake ruptures: Nature, v. 444, no. 7117, p. 358–360, doi: 10.1038/nature05275.

Yang, H., Moresi, L. N., & Quigley, M., 2020, Fault spacing in continental strike-slip shear zones : Earth and Planetary Science Letters, v. 530, doi : 10.1016/j.epsl.2019.115906.

Zuza, A.V., Yin, A., Lin, J., Sun, M., 2017, Spacing and strength of active continental strike-slip faults: Earth and Planetary Science Letters, v. 457, p. 49–62, doi: 10.1016/j.epsl.2016.09.041.

ACKNOWLEDGEMENTS

We thank Bertrand Maillot for his insights during experiments and result analyses. M. Cook, H. Yang, and an anonymous reviewer helped improve significantly this manuscript. This work has been partly funded by ANR project Geosmec (ANR-12-BS06-0016).

FIGURES

Figure 1: **a.** Surface rupture map of the 1992 Landers earthquake, California. Segmentation (black lines), according to Klinger (2010). **b.** Evolutionary scheme of the formation of strike-slip faults, seen from the surface, and a 3D sketch to illustrate the helicoidal-shape of the Riedels. **c.** Top view of the sandbox, with the measured parameters, S: inter-Riedel distance, L: Riedel length, α: angle between the Riedel and the basement fault.

Figure 2: Comparison between inter-Riedel distance (S) and sandpack thickness (T) for different frictional and cohesional properties of the sand. **a.** Pictures of the top of the sandbox

after ~11-12 mm of displacement for experiments with a 2, 3 and 4 cm-thick sandpack. **b., c., d., e.** Average inter-Riedel distance (S) per experiment versus sand-pack thickness (T) for Sand 1 (b.); for three different sands with different internal friction (**c**); for three different basal materials to study the basal friction effect (**d**); and for two sands with different cohesion (**e**). Note that for clarity's sake, for Sand 1 on graphics **c** and **d**, we represent the average value by thickness rather than by experiment.

Figure 3 : Normalised length of individual fault segments for several continental strike-slip earthquakes (Klinger, 2010, Lauer et al., 2018) and for individual analogue-fault segments. Sand 1 is shown only for comparison. The length is normalized to inferred seismogenic thickness or sand thickness accordingly. Values of seismogenic crust thicknesses are estimated from the literature (see Supp. Mat.)

Figure 4: **a.** Curl of the incremental displacement field for a 4 cm-thick experiment (T=4cm) at three different stages of the deformation (d=7.5mm, d=10mm, d=13mm). The curl is derived from the correlation image between two successive pictures of the sandbox surface. It highlights the location of shear. The location of the different active faults (R-shear, S-shear) is highlighted. **b.** Scheme of the 3D-structures of a strike-slip fault at the crustal scale.

Figure 3 : Normalised length of individual fault segments for several continental strike-slip earthquakes (Klinger, 2010, Lauer et al., 2018) and for individual analogue-fault segments (see Fig. S13 for comparison with sands 1 and 4). The length is normalized to inferred seismogenic thickness or sand thickness accordingly. Values of seismogenic crust thicknesses are estimated from the literature (see Supp. Mat.)

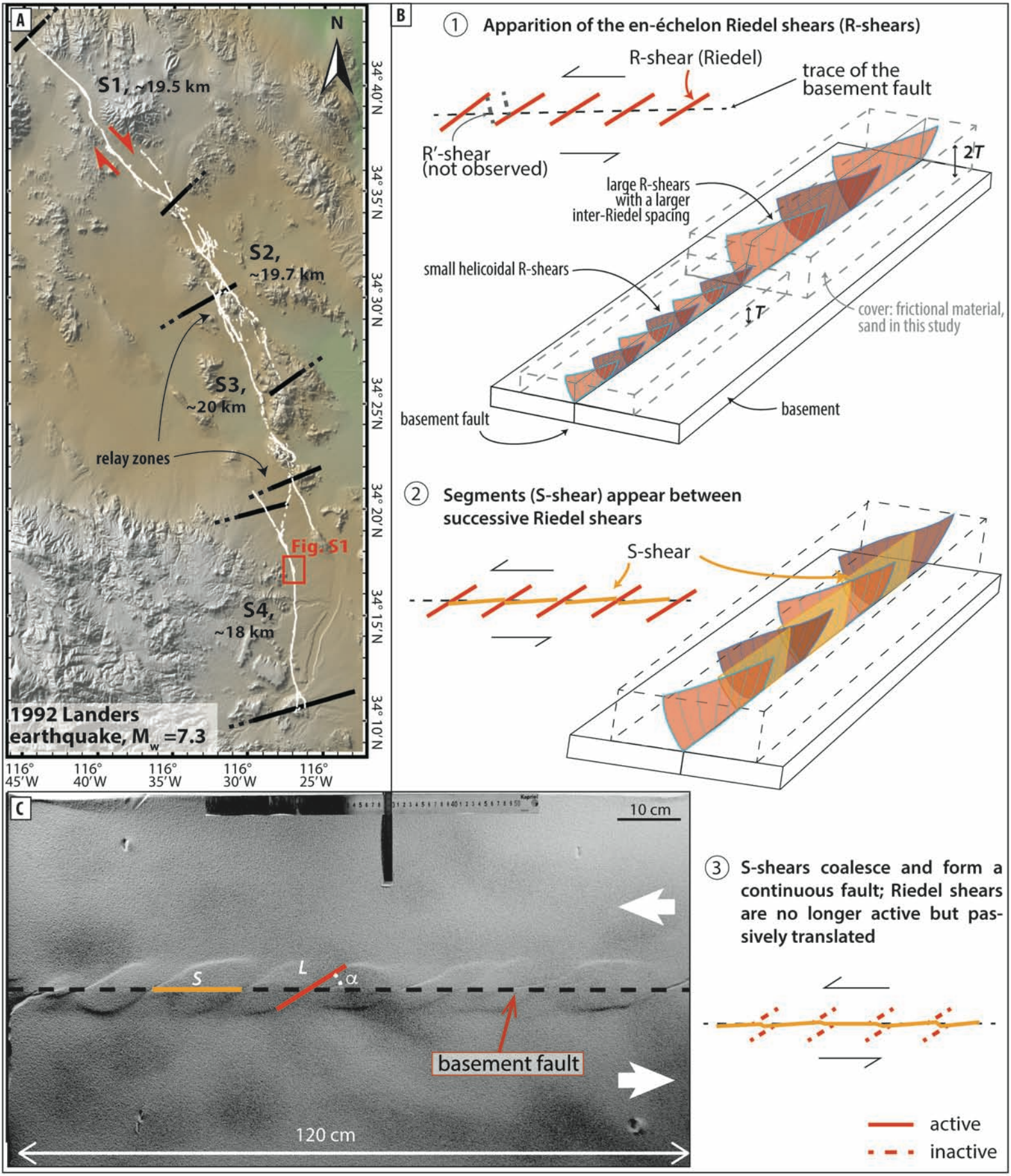
A
N
S1, ~19.5 km
S2, ~19.7 km
S3, ~20 km
S4, ~18 km
relay zones
Fig. S1
1992 Landers earthquake, Mw =7.3
34° 40'N
34° 35'N
34° 30'N
34° 25'N
34° 20'N
34° 15'N
34° 10'N
116° 45'W
116° 40'W
116° 35'W
116° 30'W
116° 25'W
B
① Apparition of the en-échelon Riedel shears (R-shears)
R-shear (Riedel)
trace of the basement fault
R'-shear (not observed)
2T
large R-shears with a larger inter-Riedel spacing
small helicoidal R-shears
T
cover: frictional material, sand in this study
basement fault
basement
② Segments (S-shear) appear between successive Riedel shears
S-shear
C
10 cm
S
L
α
basement fault
120 cm
③ S-shears coalesce and form a continuous fault; Riedel shears are no longer active but passively translated
active
inactive

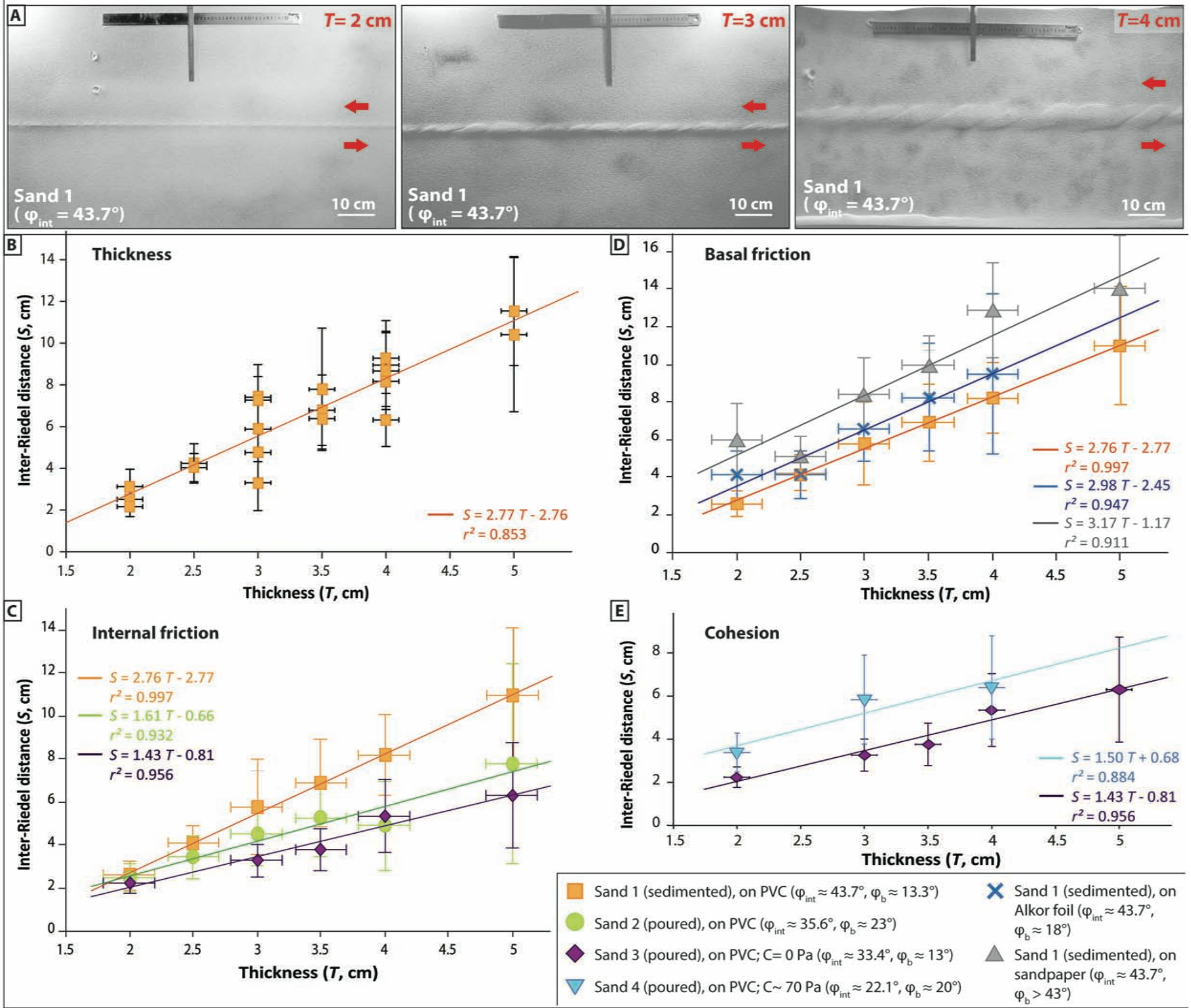
A
T= 2 cm
Sand 1
(φint = 43.7°)
10 cm
T=3 cm
Sand 1
(φint = 43.7°)
10 cm
T=4 cm
Sand 1
(φint = 43.7°)
10 cm
B
Thickness
Inter-Riedel distance (S, cm)
Thickness (T, cm)
S = 2.77 T - 2.76
r² = 0.853
D
Basal friction
Inter-Riedel distance (S, cm)
Thickness (T, cm)
S = 2.76 T - 2.77
r² = 0.997
S = 2.98 T - 2.45
r² = 0.947
S = 3.17 T - 1.17
r² = 0.911
C
Internal friction
Inter-Riedel distance (S, cm)
Thickness (T, cm)
S = 2.76 T - 2.77
r² = 0.997
S = 1.61 T - 0.66
r² = 0.932
S = 1.43 T - 0.81
r² = 0.956
E
Cohesion
Inter-Riedel distance (S, cm)
Thickness (T, cm)
S = 1.50 T + 0.68
r² = 0.884
S = 1.43 T - 0.81
r² = 0.956
Sand 1 (sedimented), on PVC (φint ≈ 43.7°, φb ≈ 13.3°)
Sand 2 (poured), on PVC (φint ≈ 35.6°, φb ≈ 23°)
Sand 3 (poured), on PVC; C= 0 Pa (φint ≈ 33.4°, φb ≈ 13°)
Sand 4 (poured), on PVC; C~ 70 Pa (φint ≈ 22.1°, φb ≈ 20°)
Sand 1 (sedimented), on Alkor foil (φint ≈ 43.7°, φb ≈ 18°)
Sand 1 (sedimented), on sandpaper (φint ≈ 43.7°, φb > 43°)

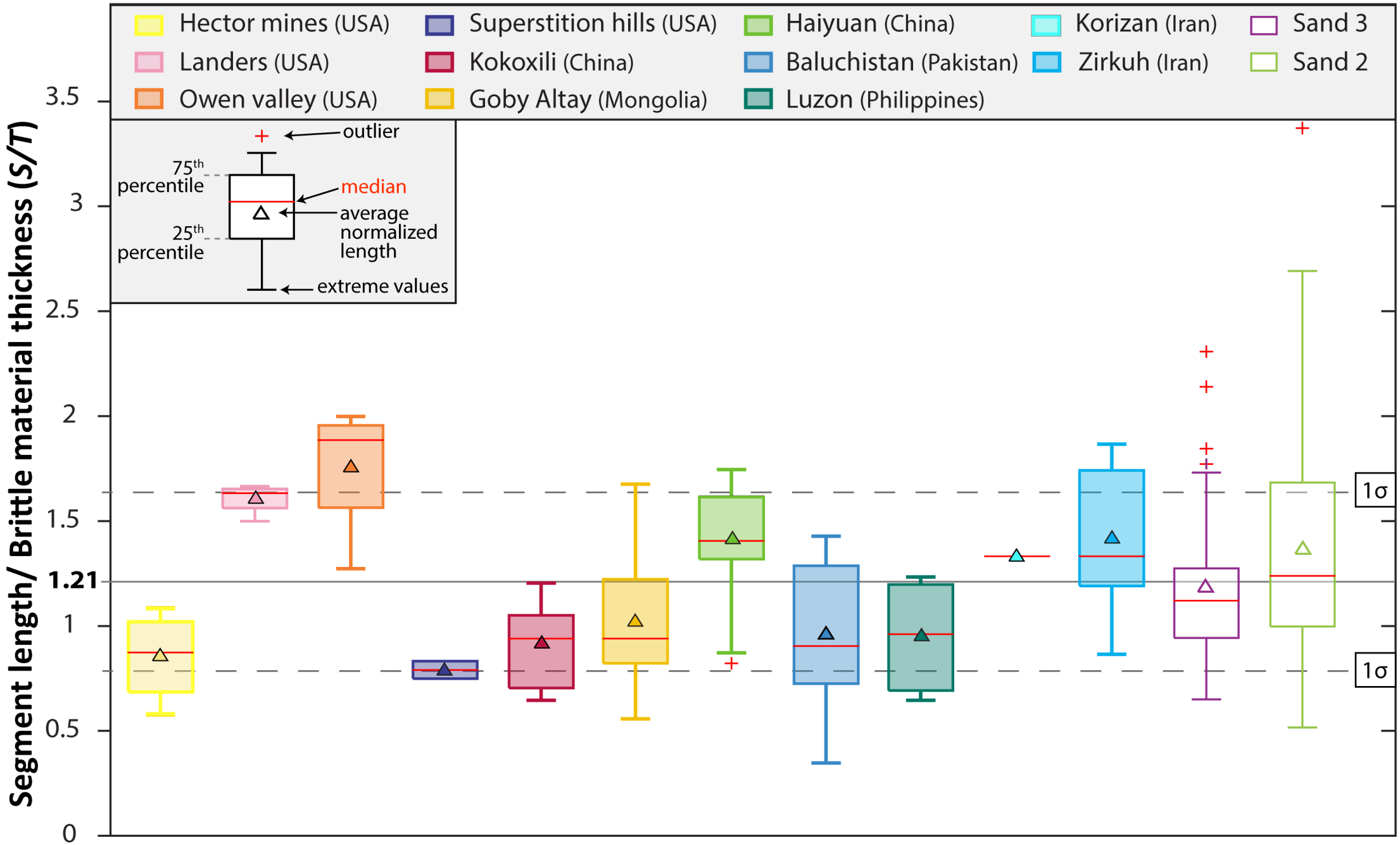
Hector mines (USA)
Landers (USA)
Owen valley (USA)
Superstition hills (USA)
Kokoxili (China)
Goby Altay (Mongolia)
Haiyuan (China)
Baluchistan (Pakistan)
Luzon (Philippines)
Korizan (Iran)
Zirkuh (Iran)
Sand 3
Sand 2
outlier
75th percentile
median
average normalized length
25th percentile
extreme values
Segment length/ Brittle material thickness (S/T)
3.5
3
2.5
2
1.5
1.21
1
0.5
0
1σ
1σ

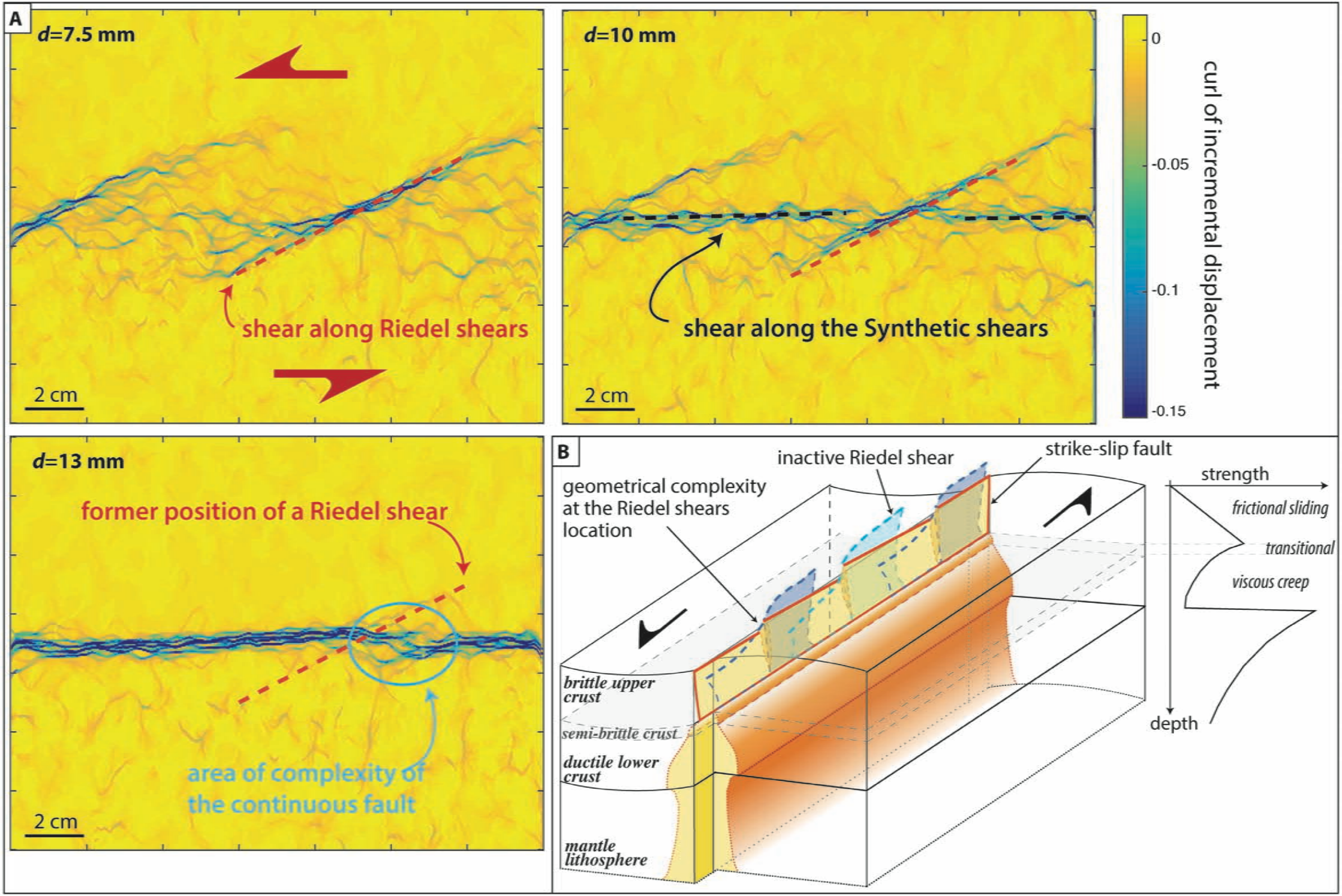
A
d=7.5 mm
shear along Riedel shears
2 cm
d=10 mm
shear along the Synthetic shears
2 cm
0
-0.05
-0.1
-0.15
curl of incremental displacement
d=13 mm
former position of a Riedel shear
area of complexity of the continuous fault
2 cm
B
inactive Riedel shear
strike-slip fault
geometrical complexity at the Riedel shears location
brittle upper crust
semi-brittle crust
ductile lower crust
mantle lithosphere
strength
frictional sliding
transitional
viscous creep
depth